Journal Pre-proofs

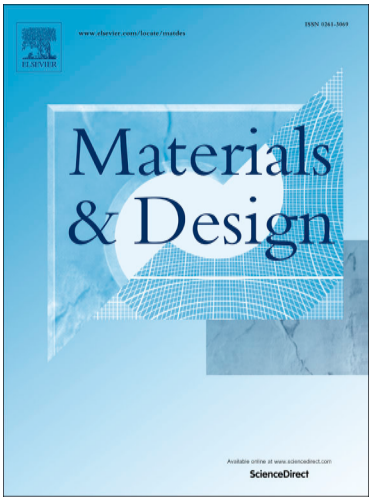

Microstructural evolution and mechanical properties of CuSn5 processed by HPT followed by short-time annealing

Yuting Dai, Ali Ahmadian, Oliver Petry, Marcel Sos, Matthias Schwotzer, Karsten Durst, Christian Kübel

PII: S0264-1275(25)01317-6
DOI: https://doi.org/10.1016/j.matdes.2025.114897
Reference: JMADE 114897

To appear in: *Materials & Design*

Received Date: 26 May 2025
Revised Date: 31 August 2025
Accepted Date: 6 October 2025

Please cite this article as: Dai, Y., Ahmadian, A., Petry, O., Sos, M., Schwotzer, M., Durst, K., Kübel, C., Microstructural evolution and mechanical properties of CuSn5 processed by HPT followed by short-time annealing, *Materials & Design* (2025), doi: https://doi.org/10.1016/j.matdes.2025.114897

Microstructural evolution and mechanical properties of CuSn5 processed by HPT followed by short-time annealing

Yuting Dai[1,2]; Ali Ahmadian[1,3,4]; Oliver Petry[5]; Marcel Sos[5]; Matthias Schwotzer[6]; Karsten Durst[5]; Christian Kübel[1,2,3,4]

[1]Institute of Nanotechnology (INT), Karlsruhe Institute of Technology, Hermann-von-Helmholtz-Platz 1, 76344, Eggenstein-Leopoldshafen, Germany

[2]In-situ Electron Microscopy, Department of Materials and Earth Sciences, Technical University of Darmstadt, Peter-Grünberg-Straße 2, 64287, Darmstadt, Germany

[3]Helmholtz Institute Ulm for Electrochemical Energy Storage (HIU), Albert-Einstein-Allee 11, 89081, Ulm, Germany

[4]Karlsruhe Nano Micro Facility (KNMFi), Karlsruhe Institute of Technology, Hermann-von-Helmholtz-Platz 1, 76344, Eggenstein-Leopoldshafen, Germany

[5]Physical Metallurgy, Department of Materials and Earth Sciences Technical University of Darmstadt, Darmstadt, Peter-Grünberg-Straße 2, 64287, Darmstadt, Germany

[6]Institute of Functional Interfaces (IFG), Karlsruhe Institute of Technology, Hermann-von-Helmholtz-Platz 1, 76344, Eggenstein-Leopoldshafen, Germany

Abstract:

Nanocrystalline and ultrafine-grained metallic materials have received considerable attention in recent years due to their ultrahigh strength and unique mechanical properties. However, pure nanocrystalline metals exhibit thermal instability, making them prone to grain growth during thermal treatment and usage, which in turn reduces hardness and strength, and compromises their structural integrity. To improve the thermal stability of these materials, grain boundary segregation of solute elements has emerged as a promising approach. In this study, we used advanced scanning transmission electron microscopy to investigate the grain growth

mechanisms of ultrafine-grained Cu-5 wt.% Sn annealed at temperatures up to 350 °C. Our results indicate that Sn preferentially segregates at general high-angle GBs, while low-angle and coincidence site lattice GBs do not exhibit detectable enrichment of Sn. The segregation at these high angle GBs and GB relaxation explains the increased Vickers hardness of the Cu-Sn alloy during annealing.

Keywords:

Ultrafine-grained microstructure; annealing induced hardening; grain boundary segregation; 4D-STEM; grain growth;

1. Introduction

Grain boundaries (GBs) play a crucial role in determining both mechanical and thermal properties of polycrystalline materials. It is well known that GBs act as barriers to dislocation motion, which leads to the strengthening of polycrystalline materials. The relationship between the fraction of GBs or the grain size and the strength is described by the Hall-Petch equation [1, 2]. Reducing the grain size in ultrafine-grained (UFG) materials results in an increase in strength. The grain size reduction can be achieved by severe plastic deformation (SPD) [3] techniques, such as high-pressure torsion (HPT) [4-6]. For pure copper (Cu) it has been shown that the strength can be increased by 300% by HPT processing [7]. Furthermore, it has been shown that solid solution hardening influences the saturation grain size achieved after HPT. In alloy systems such as CuSn and CuZn, those with the highest solid solution hardening exhibit the smallest saturation grain size, independent of their stacking fault energy, indicating that atomic size and modulus mismatch effects dominate over SFE in controlling grain refinement [8-10].

While grain refinement of Cu by HPT enhances its strength and hardness, temperature-driven grain growth gradually reverses the effect, leading to a decrease in strength. Huang et al. [7] reported grain growth of high-purity UFG-Cu even at room temperature. They concluded a correlation between the self-annealing and the number of HPT turns. For less than one turn (N<=1) abnormal grain growth occurs, while for a high number of turns (N>5), the grain size and hardness remain stable from 48h to 4 weeks. Edalati et al. [11] prepared Cu using HPT at 100 K and 300 K, Cu processed at 100 K had an average grain size of ~80 nm, while Cu processed at 300 K has an average grain size of ~300 nm. However, samples processed at 100 K exhibited self-annealing within hours, progressing faster at higher shear strains due to a high density of lattice defects. In a complementary study, Liang et al. [12] used thermodynamic calculations of stored energy and kinetic measurements of the activation energy for

recrystallization to investigate thermal stability of Cu. The results indicate that the presence of a higher proportion of low-angle GBs (LAGB) in Cu contributes to its enhanced thermal stability. This is because LAGBs have a higher activation energy and exhibit lower mobility compared to high-angle GBs (HAGB), thereby slowing down the recrystallization process. Schafler et al. [13] examined the effect of temperature on grain size and hardness in high-purity UFG-Cu annealed after HPT. Up to 134 °C (0.3 T/Tm), partial recrystallization occurs, which leads to a decrease in hardness by about 10% due to the partial recrystallization and dislocation recovery. At higher temperatures, full recrystallization occurs, leading to significant grain growth and substantial decrease in strength. The thermal stability of the UFG Cu-X alloy series was also found to be strongly influenced by the solid solution strengthening. Even though CuSn5 has the smallest saturation grain size, it exhibits a better thermal stability after annealing [10, 14].

In order to prevent grain growth in UFG-Cu, it has been suggested to introduce alloying elements at the grain boundaries, as the grain growth is linked to GB migration [15]. By engineering the structure and composition of the grain boundaries, thermally assisted grain growth can be reduced [16]. Prominent candidates to stabilize UFG-Cu are zirconium (Zr) [17] , tantalum (Ta) [18] and tin (Sn) [19] because of their low solubility in Cu. Atwater et al. [17] reported that only 1 at% Zr is sufficient to stabilize the nanocrystalline Cu by forming small intermetallic phases at the GBs. However, it should be mentioned that CuZr-alloys possess a high glass-forming ability [20] and therefore, the segregation of Zr at the GB would result in the formation of an amorphous intergranular film after annealing at high temperatures (850°C), as demonstrated by Khalajhedayati et al. [21]. In both cases, the Zr segregation lowers the boundary energy and impedes GB migration. Besides phase transformation or glass formation of the GB, GB precipitation is also known to reduce migrating GBs by Zener pinning [22].

The addition of 8 wt.% Sn to Cu improves the mechanical properties by increasing the GB strength and the recrystallization temperature by 100 °C. Differential scanning calorimetry (DSC) measurements by Zaher et al. [19] showed that the activation energy for recrystallization in Cu-8 wt.% Sn is significantly higher (200 kJ/mol) than in pure Cu (92 kJ/mol). They attributed this to strong interactions between Sn solute atoms and crystalline defects, particularly dislocations and GBs, which slow down the recrystallization kinetics. However, the studies did not focus on the actual composition at GBs. In particular, there is no classification of which GBs are preferred for Sn segregation. Therefore, it is crucial to understand which GBs are influenced by Sn segregation and whether potentially a phase transformation occurs at the interfaces.

In this study, we investigate the thermal stability of ultrafine-grained Cu-5 wt.% Sn (CuSn5) alloys, focusing on grain growth and cell parameters during annealing at temperatures up to 350 °C. We employ differential scanning calorimetry (DSC) and X-ray diffraction (XRD) to assess these thermal stability characteristics. Additionally, advanced scanning transmission electron microscopy (STEM) techniques, including energy dispersive X-ray spectroscopy (EDX) and 4D-STEM with precession electron diffraction (PED) for orientation mapping (ACOM), are utilized to analyze various types of grain boundaries (GBs), such as low-angle GBs, high-angle GBs, and twin boundaries, revealing a distinct segregation behavior. Our findings indicate that Sn only segregates to general HAGBs and enhances the stability of the grain structure, while twin boundaries and LAGBs are not enriched with Sn. Furthermore, comparative studies on coarse-grained CuSn5 revealed that the driving force for Sn segregation is not influenced by HPT.

2.Experimental Methodology

HPT samples with a diameter of 20 mm and an initial height of 4 mm were prepared from CuSn5 rods (average grain size: 30 ± 11 μm, as shown in Supplementary Fig. S1) provided by Wieland-Werke AG (Germany). The HPT anvils had a cavity diameter of 20 mm and height of 1.5 mm each. A pressure of 4.6 GPa was applied for 30 rotations with a speed of 1 rpm using an HPT press by W. Klement GmbH (Austria). A cooling ring was mounted to the upper anvil to keep the process temperature close to ambient. The deformed samples were used for isochronal annealing at various temperatures from 100 to 350 °C for 1 h.

Specimens for X-ray diffraction (XRD) analysis were prepared by mechanical polishing and final electro-polishing using D2 electrolyte (from Struers) at 7 V and -20 °C to remove the deformed surface layer. The crystal structure of all samples was determined by XRD using (Malvern Panalytical) using Cu Kα radiation at 40 kV and 40 mA. The lattice parameter a , was calculated via Rietveld refinement using the Highscore software v. 5.1b.

Vickers micro-hardness measurements were done using a Buehler Micromet-5104 device with a load of 300 g and a dwell time of 10 s on the polished surface of the samples. The distance between each indent was 0.5 mm and at least 30 indents were measured.

Nanoindentation testing was conducted using an Agilent G200 nanoindentation system equipped with a diamond Berkovich tip (Synton-MDP). The hardness and indentation modulus were measured in continuous stiffness measurement mode (CSM) at a frequency of 45 Hz using an indentation strain rate of 0.05 s^{-1}, averaging the data in an indentation depth interval between 1000 to 2000 nm. An Olympus LEXT OLS4100 confocal laser scanning microscope was used

to measure the surface topography afterwards. The pile-up height was determined in relation to the surrounding flat surface.

The microstructure of the as-cast coarse-grained CuSn5 (CG-CuSn5) was characterized by electron backscatter diffraction (EBSD) using a Zeiss Auriga 60 dual beam operated at 20 kV and equipped with a EDAX EBSD detector. Sample preparation for EBSD was performed following the same procedure as used for XRD. The EBSD data were analyzed with EDAX OIM analysis 8 software.

TEM specimens were prepared using a FEI Strata 400S focused ion beam/scanning electron microscope (FIB/SEM) system to investigate the microstructure in (SD, RD) plane, as shown in Supplementary Fig. S2. Annular dark-field STEM (ADF-STEM) images were acquired on an aberration (probe) corrected Titan Themis 300 (Thermo Fischer Scientific) operated at 300 kV using a convergence angle of 30 mrad and a camera length 245 mm. Precession electron diffraction (PED) experiments for orientation mapping (ACOM) were performed with the NanoMegas ASTAR system, using a precession angle of 0.6°. For that, the microscope was operated in micro-probe STEM mode with a convergence angle of 0.5 mrad, which results in a diffraction limited beam diameter of about 1.5 nm, and a camera length of 245 mm. The diffraction pattern were acquired with a pixelated detector (Dectris Quadro) and the step size as well as acquisition time for the different samples were: as-HPT CuSn5 and HPT-CuSn5 200 °C (step size 2 nm, acquisition time 250 s), HPT-CuSn5 300 °C (3 nm, 640 s) and HPT-CuSn5 350 °C (5 nm, 360 s).

3. Results

3.1 Mechanical properties

In order to study the thermal stability of the HPT-processed CuSn5 alloy, microhardness measurements were performed on as-received coarse-grained (as-CG) CuSn5, HPT-processed (as-HPT) and subsequently annealed at various temperatures, as shown in Fig. 1. The as-CG sample showed a hardness of 88 HV. After HPT, the hardness increased significantly by a factor of 4, reaching 316 HV. After annealing to 100 °C, the hardness increased further to 335 HV, representing an increase of 6 %. With further annealing at 200 °C, the hardness increased more to 349 HV, reflecting a 10 % rise compared to the as-HPT sample. However, upon annealing at 300 °C, the hardness started to decrease to 313 HV. When the annealing temperature reached 350 °C, the hardness decreased further to 214 HV. The Vickers indentation induced slight pile-up formation (Supplementary Fig. S3) around the indent. However, the pile-up formation was very comparable at RT and 200°C, suggesting that the observed increase in hardness from RT to 200 °C is a true materials property and not due to pile-up formation. This was further

confirmed using nanoindentation. As shown in the Fig. 1(b), the Oliver-Pharr method indicated an increase in hardness from 4.06 GPa at room temperature to 4.61 GPa after annealing at 200 °C, with pile-up height increased slightly from 0.21 ± 0.04 µm to 0.33 ± 0.09 µm. Additionally, the harmonic contact stiffness from continuous stiffness measurements (CSM) was used to accurately determine the contact area via Sneddon's equation [23]. With this, the calibrated hardness increased from 3.95 GPa at RT to 4.10 GPa after annealing at 200 °C.

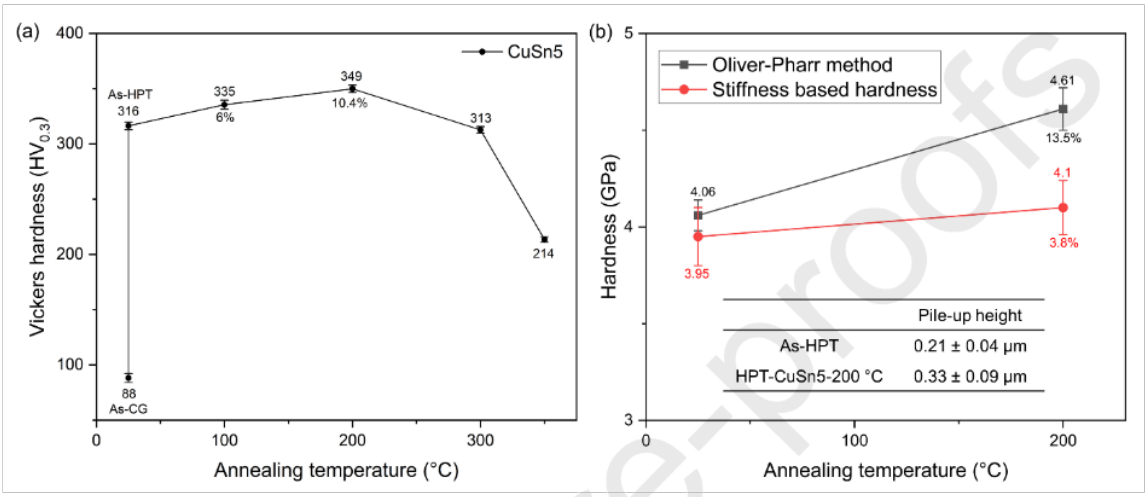

Figure 1:(a) Evolution of hardness in CuSn5 after HPT and subsequent annealing at 100 °C, 200 °C, 300 °C,250 °C and 350 °C for 1h showing a maximum hardness at 200 °C; (b) Nanoindentation hardness measurements performed on as-HPT and an annealed HPT sample (200 °C for 1 h)

3.2 Microstructural evolution during isothermal annealing

3.2.1 XRD analysis

To further explore the observed changes in hardness and confirm their relationship to microstructural stability, XRD analysis was conducted on both as-deformed and annealed samples. The XRD patterns for the CuSn5 sample for the different conditions (as-CG, as-HPT, HPT+annealing) are shown in Fig. 2(a). Peaks belonging to the (111), (200), (220), (311) and (222) FCC planes are indicated. It should be highlighted that both the HPT processing (as-HPT) as well as the annealing did not result in the formation of any secondary phases, indicating that all samples retained an FCC crystal structure in a single solid-state solution phase.

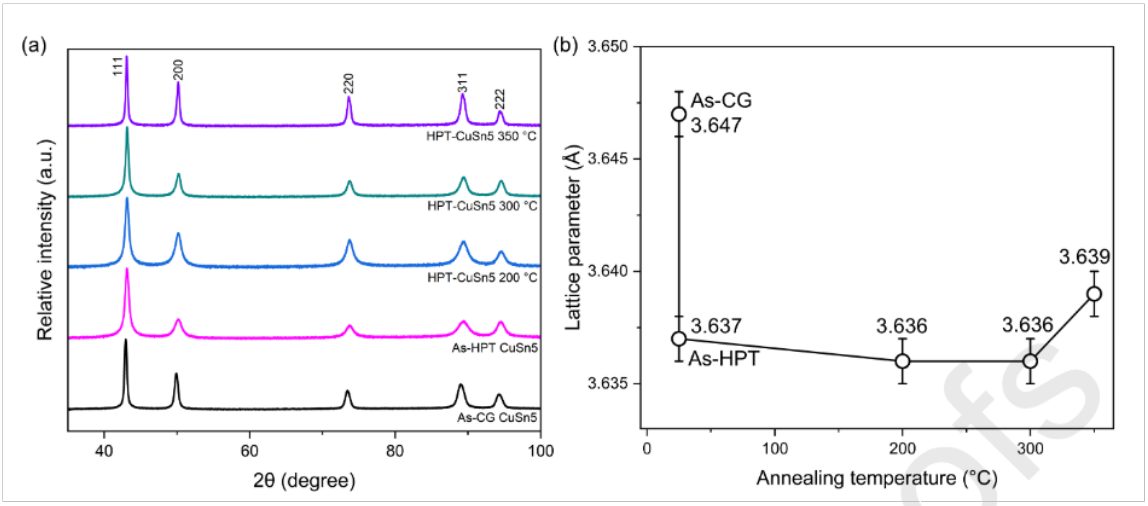

Figure 2: (a) XRD analysis of the as-CG, as- HPT and HPT+annealing at 200 °C, 300 °C and 350 °C CuSn5 samples showing a single FCC-Cu phase. (b) Variation of lattice parameter with annealing temperature indicates a significant reduction after HPT. Subsequent annealing up to 300 °C results in no noticeable changes, while annealing at 350 °C leads to an increase of the lattice parameter.

Fig. 2(b) reveals a decrease in the lattice parameter a from initially 3.647 Å to 3.637 Å after HPT, which is mainly due to segregation of dissolved Sn at new GBs as will be discussed in detail later and possibly minor contributions due to compressive stress fields inside grains originating from non-equilibrium GBs [24]. The following annealing caused minor changes and a slight increase to 3.639 Å at 350 °C.

3.2.2 TEM analysis

While XRD confirmed the presence of a single-phase FCC structure before and after annealing, detailed knowledge on the grain size distribution, possible segregations at grain boundaries and relative misorientation was obtained from STEM analysis.

Electron backscatter diffraction (EBSD) revealed an average grain size of 30 µm (see Supplementary Fig. S1) for the initial coarse-grained polycrystalline CuSn5. After HPT the grain size was reduced significantly. ADF-STEM images of CuSn5 after HPT and after annealing at 200 °C, 300 °C, and 350 °C are presented in Fig. 3(a-d). The corresponding orientation maps (IPF-z) show a nanocrystalline (NC) microstructure with a grain size (area weighted) of 91 ± 52 nm after HPT, as shown in Fig. 3(e). The ADF-STEM image and quantitative analysis in Figs. 3(b) and (f) show that annealing at 200 °C resulted to a grain size of 87 ± 47 nm (see table 1) with a low dislocation density observed inside the grains. This indicates that during annealing up to 200 °C grain growth did not take place. However, the first exothermic peak observed in the DSC thermogram (see Supplementary Fig. S8) together with

the reduction of the LAGB fraction (table 1) indicates that stress relaxation processes occur at the grain boundaries and contribute to the hardening of the NC CuSn5. After further annealing at 300 °C, a bimodal microstructure start to develop, as shown in Fig. 3(c). This bimodal microstructural evolution fits the observed reduction in hardness, confirming the influence of grain size on the material's mechanical properties. Increasing the annealing temperature to 350 °C leads to further coarsening of the microstructure, as depicted in Fig. 3(d). The thermal stability of CuSn5 up to 200 °C, as well as the bimodal coarsening of the microstructure are in agreement with high temperature scanning indentation experiments performed by Sos et al. [25].

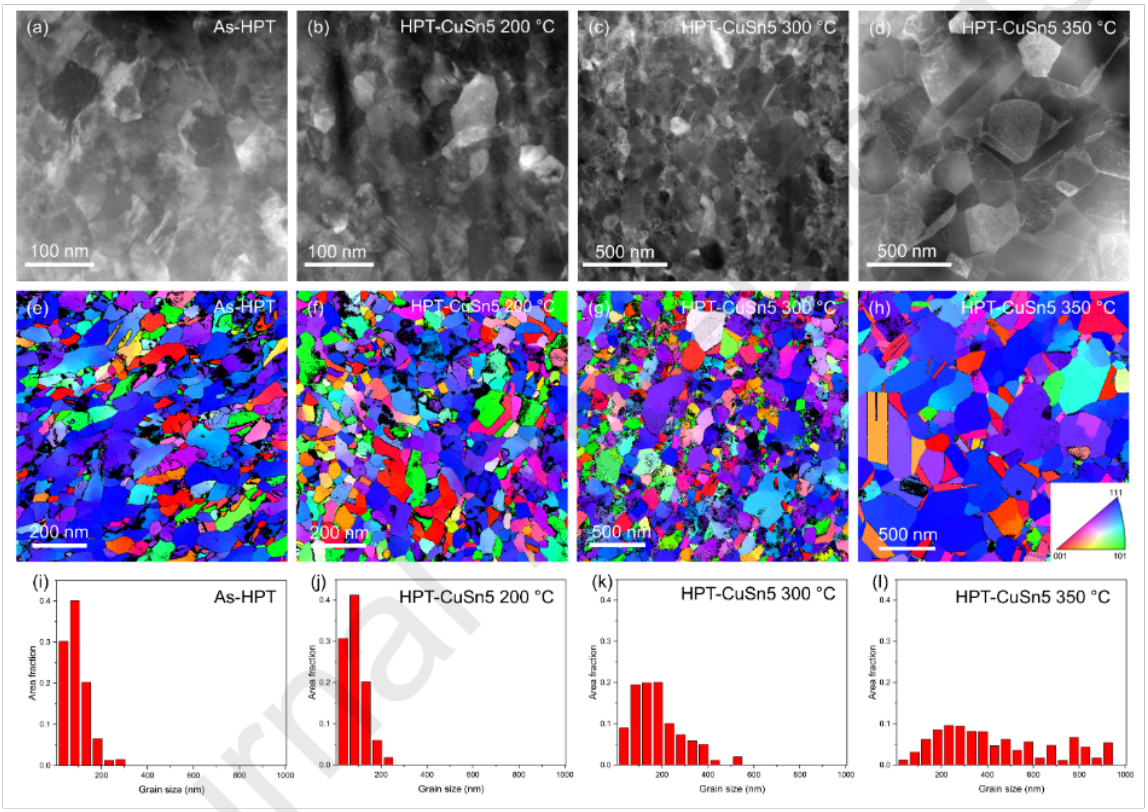

Figure 3: ADF-STEM (top row), ACOM maps (middle row) and corresponding grain size distributions (bottom row) of CuSn5 at various post-HPT annealing conditions: (a/e/i) at room temperature, (b/f/j) annealed at 200 °C, (c/g/k) annealed at 300 °C, and (d/h/l) annealed at 350 °C. While the ADF-STEM and ACOM maps qualitatively illustrate the microstructural evolution, the grain size distributions provide insight into the thermal stability and coarsening behavior with increasing annealing temperature.

In order to get more insights into the change of the microstructure, PED based ACOM was used to characterize the orientation distribution and the fraction of LAGBs, HAGBs and CSL (coincidence site lattice) boundaries. For a reliable quantitative analysis of the microstructure, a modified version of the procedure reported by Kobler et al. [26, 27] was employed. As shown

in Fig. 3(e), the as-HPT sample consisted of equiaxed nanocrystalline grains with a (111) dominated orientation distribution. As the annealing temperature increased, the grain size was found to increase in Fig. 3(g) and (h), in agreement with the ADF-STEM analysis, while the orientation of the individual grains still exhibited a preference for the (111) orientation.

The comparison of Fig. 3(j) and Fig. 3(k) clearly shows the microstructural evolution of CuSn5 between 200 °C and 300 °C. When processed at 300 °C, the material exhibited significant grain growth, forming a microstructure composed of a nanocrystalline matrix and coarsened grains ranging from 200 nm to 520 nm. Table 1 summarizes the results. As discussed before, the grain growth was inhibited up to 200 °C with an average grain size of ≈ 90 nm, but increased significantly at higher temperatures. After annealing at 200 °C for 1 h, the fraction of LAGBs decreased slightly from 17% to 14 %, despite the absence of grain growth. However, this trend reversed when the annealing temperature increases to 300 °C, where the LAGB fraction rose to 19% accompanied with the onset of grain growth. The slight increase in the fraction of LAGBs can be explained following the idea by J. Duan et al. [28]: LAGBs have lower mobility and energy, so they remain relatively stable. As a result, grains surrounded by HAGBs grow faster and are preferentially consumed, which leads to an increase in the LAGB fraction. In addition, ACOM revealed some subgrain structures within the coarsened grain interiors, as indicated by the LAGBs in Supplementary Fig. S4. The fraction of HAGBs increased at 350 °C, which implies a high degree of recrystallization. The fraction of Σ3 twin boundaries, corresponding to annealing twins, significantly increased at 350 °C.

Table 1 Structural parameters of HPT CuSn5 subjected to annealing at 200°C, 300°C and 350°C for 1h

	LAGB fraction (%)	Σ 3 fraction (%)	Other HAGB fraction (%)	Area weighted grain size (nm)
As-HPT CuSn5	17±1	10±1	73±1	91±52
HPT-CuSn5-200 °C	14±1	10±1	76±1	87±47
HPT-CuSn5-300 °C	19±2	11±2	70±2	173±95
HPT-CuSn5-350 °C	10	26	64	462±268

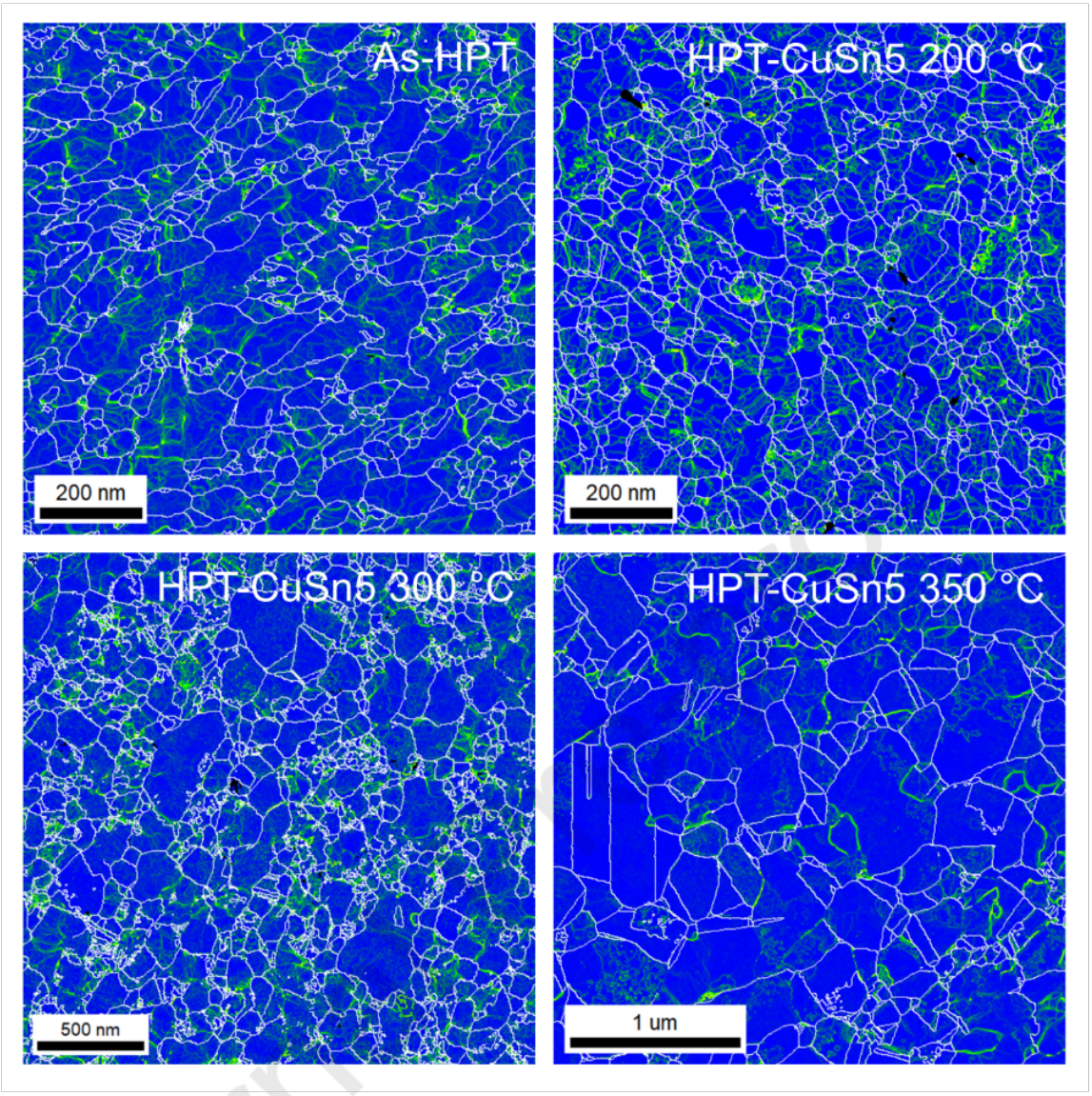

Figure 4: KAM maps of CuSn5 at various conditions: (a) as-HPT, (b) annealed at 200 °C, (c) annealed at 300 °C, and (d) annealed at 350 °C.

Fig. 4 shows the KAM maps for CuSn5 at various states. No significant differences are observed between the as-HPT sample and the specimen annealed at 200 °C. After annealing at 300 °C, however, the KAM maps reveal clear signs of initial microstructural evolution, particularly the appearance of some relatively larger grains similar to those in the specimen annealed at 350 °C.

3.2.3 Solute segregation

The XRD and STEM results indicate that no secondary phase or particles were formed before and after annealing treatment. Solute atoms however can segregate to defects such as dislocations, stacking faults and grain boundaries and these segregations can cause annealing hardening [29]. In order to further understand the local chemical changes in CuSn5, STEM-

EDS measurements were performed for the different states after HPT and after annealing at different temperatures, as shown in Fig. 5. The STEM-EDS composition maps show that there is obvious Sn segregation at GBs for the HPT deformed CuSn5 as shown in Fig. 5(a-d). After annealing at 200 °C, some GBs are enriched with Sn in Fig. 5(e-h). Despite annealing at 350 °C for 1 h, where grain growth occurred, noticeable Sn segregation is observed for most GBs shown in Fig. 5(o).

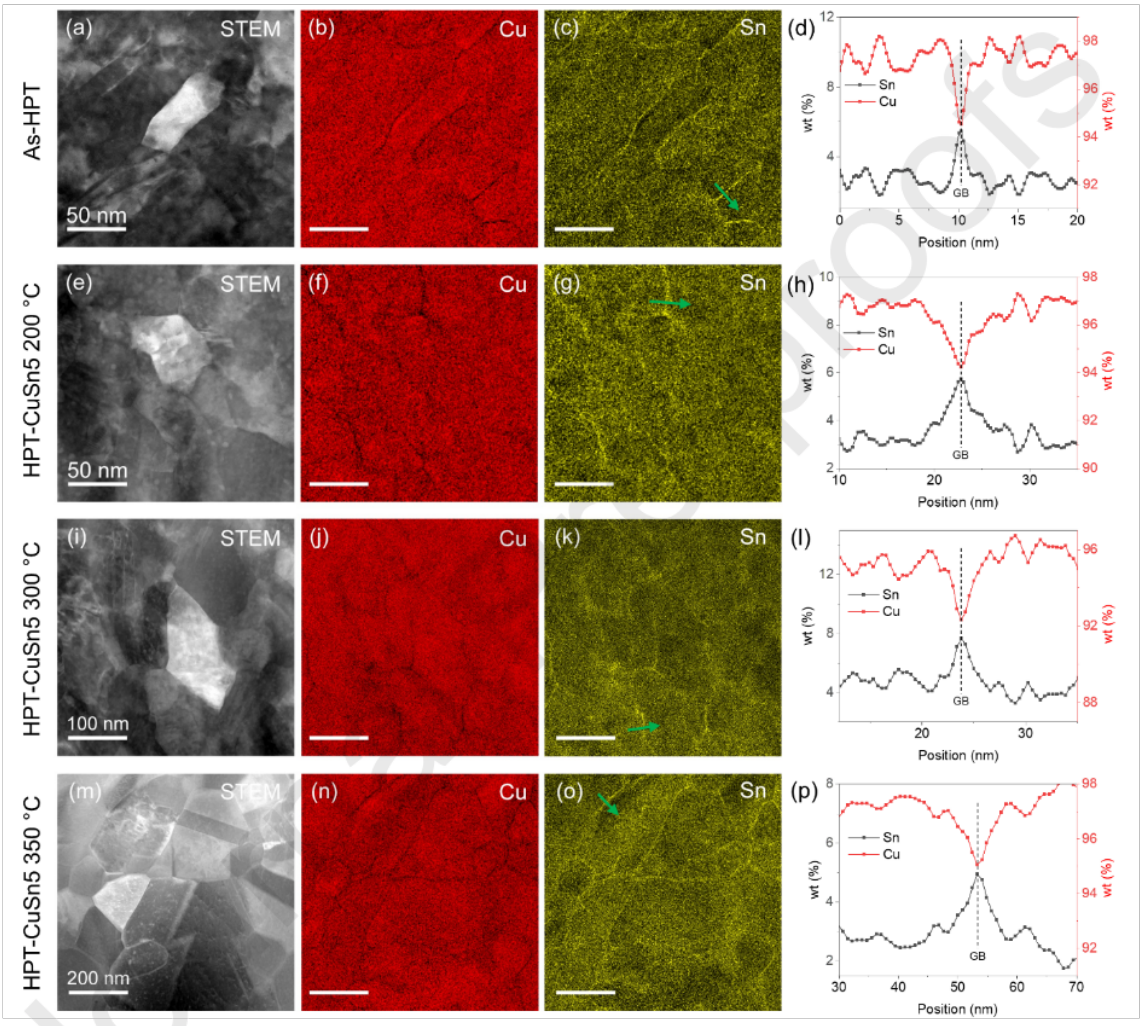

Figure 5: ADF-STEM images and corresponding STEM-EDX elemental maps of Cu and Sn, and concentration line profiles across selected GBs in CuSn5 after HPT (a-d), HPT and annealed at 200 °C (e-h), 300 °C (i-l), and 350 °C for 1h (m-p). The interfacial excess of Sn at the GBs is clearly visible throughout the annealing series.

To determine whether Sn segregation was induced by HPT, Fig. 6(a) shows the distribution of Sn along three HAGBs in the CG CuSn5 sample. The misorientation angles are 47° (grain 1-2), 52° (grain 2-3) and 52° (grain 1-3). Significant Sn segregation is observed at all three HAGBs, with a maximum concentration of 9 wt.% (~3 wt.% higher than bulk). In

contrast, Fig. 6(b) shows a CSL Σ3 twin boundary with a misorientation angle of 60 °, where no Sn segregation is observed.

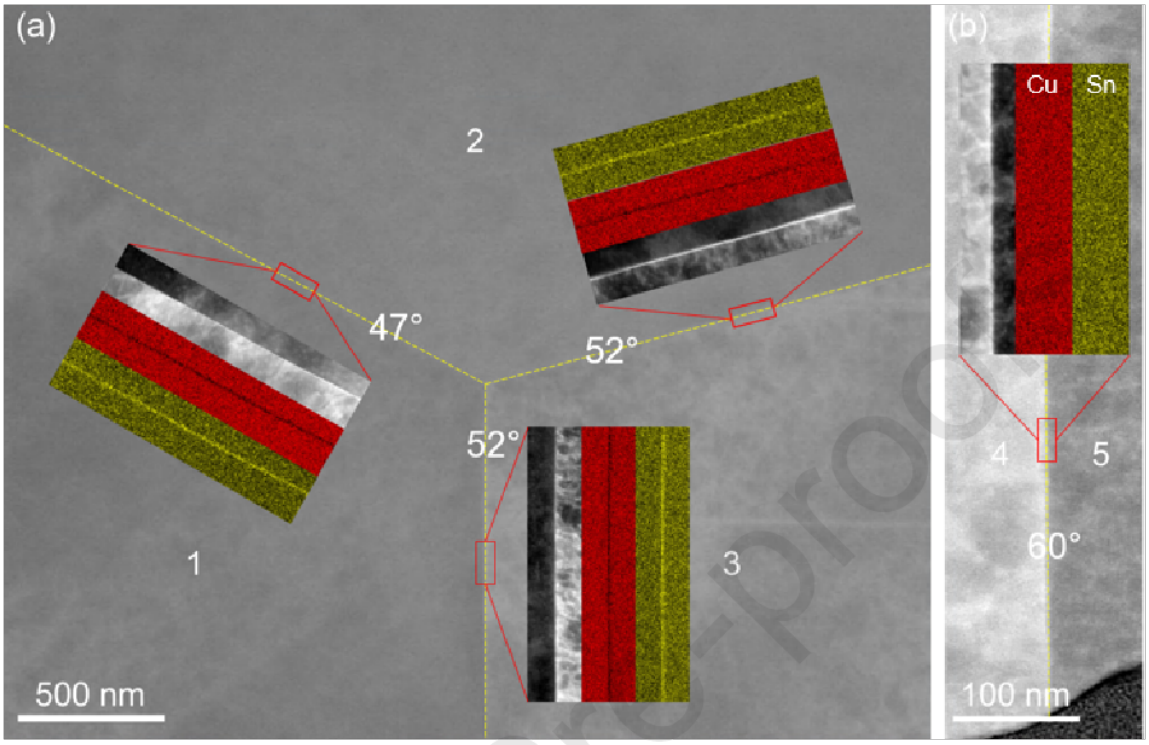

Figure 6: ADF-STEM images of CG CuSn5 and corresponding EDS maps of Cu (red) and Sn (yellow) in different misorientation angle (a) random HAGBs; (b) special twin boundary.

Moreover, based on 11 ACOM and EDX maps with more than 1000 grains analyzed, Fig. 7 displays a representative area illustrating that high-angle boundaries (indicated by black lines) are more susceptible to segregation, whereas essentially no segregation is observed along twin boundaries (marked by white lines) and only weak segregation at LAGBs (Fig. S5 and Fig. S6). Consequently, these observations further corroborate the finding that high-energy random HAGBs interact more strongly with the Sn atoms, while CSL GBs are less favorable for Sn segregation.

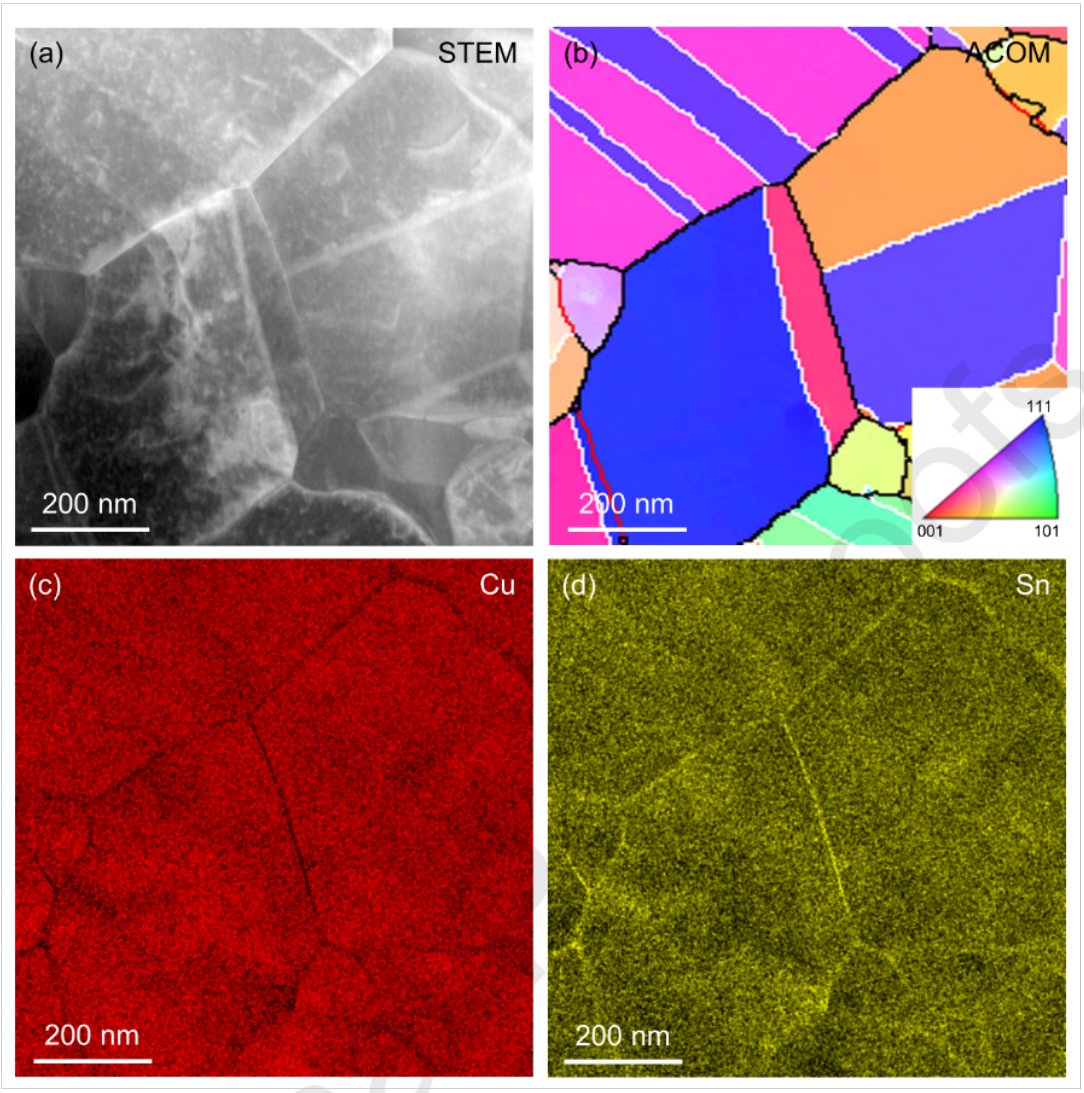

Figure 7: ADF-STEM image (a) and corresponding ACOM (b) of the same region for as-HPT CuSn5 after annealing at 350 °C for 1 hour; STEM-EDX elemental maps of Cu (c) and Sn (d) showing the GB strong segregation of Sn occurs at HAGBs (indicated by black lines) and nearly no enrichment at twin boundaries (white lines) and LAGBs (red lines).

4. Discussion

This study examined the thermal stability and hardening behavior of a HPT-processed CuSn5 alloy, focusing on the microstructural and hardness evolution upon annealing. XRD analysis revealed an unusual trend in the lattice parameter: it decreased after HPT and remained stable during annealing up to 300 °C, but increased at 350 °C. Furthermore, vickers hardness measurements revealed a notable increase in hardness after HPT, which continued up to an annealing temperature of 200 °C, after which hardness began to decline. To investigate the mechanisms underlying this behavior, STEM analyses have been performed.

The initial lattice contraction can be attributed to the significantly increased HAGB density during HPT, where the HAGBs act as sink for Sn segregation thus reducing the Sn content within the grains. This reduced Sn content results in the reduced lattice parameter. The slight increase in lattice parameter observed at 350 °C coincides with significant grain growth, reducing the density of HAGBs and thus pushing Sn back into the matrix. This behavior is similar to Cu-Zr [21] and Cu-Ta alloys [30], where solute segregation at GBs stabilized the nanostructure up to a certain temperature, after which grain growth occurred due to solute re-distribution into the matrix.

The initial hardening observed after HPT processing is consistent with the Hall-Petch hardening [1, 2], where grain refinement contributes significantly to the increased strength. Similar annealing-induced hardening effects have been reported in Cu-based alloys such as Cu-Al [31], Cu-Zn [32], Cu-Pd[33], and Cu-Au[34] and have been attributed to GB strengthening and solute segregation. In the case of CuSn5, ACOM analyses showed that the NC/UFG structure remained stable during annealing up to 200 °C, with no observable grain growth or interfacial migration (Fig. 3). This stability suggests that the hardening is not due to grain size refinement but rather is linked to other reasons. According to an overview paper by Gubicza [28], several mechanisms need to be considered to contribute to this hardening phenomenon, including: 1) annihilation of mobile dislocations and the reduction of easy dislocation sources; 2) grain boundary relaxation; 3) segregation of solute atoms to twin faults; 4) segregation of solute atoms to grain boundaries; 5) formation of twin fault; and 6) development of a “hard” texture [35].

In our case, the ACOM as shown in Fig. 3(e) and (f) revealed no significant changes in texture after annealing, ruling out the contribution of texture evolution to the hardening effect. Additionally, ACOM also did not reveal any notable change in the content of coincidence site lattice (CSL) boundaries or twins, thus discounting the influence of formation of additional twins. Different from Liu et al. [29] who observed Gd segregation at HAGBs and LAGBs after annealing treatment, STEM-EDS analysis showed that Sn segregates preferentially at HAGBs, while LAGBs and twin boundaries exhibited minimal or no Sn enrichment. The preferential segregation of Sn at HAGBs aligns with known principles of interface energy, where high-energy interfaces such as general HAGBs are more favorable for solute segregation. This behavior is similar to observations in Cu-Zr [18] alloys, where Zr segregation at HAGBs increases the stability by lowering the boundary energy and impeding GB migration. As the lattice parameters determined by XRD (Figure 2b) are essentially unchanged during annealing up to 300 °C and as the grain size is not changing up to 200 °C, this indicates that the Sn access

at the GBs is mostly unchanged during annealing up to 200 °C, suggesting that while Sn stabilizes the NC/UFG structure, it does not drive further hardening at elevated temperatures. Similar findings were reported by Khalajhedayati et al. [21], who showed that Zr segregation in nanocrystalline Cu-Zr stabilizes grain boundaries without a proportional increase in hardening effects. Furthermore, the orientation and segregation maps (Fig. 5 and 6) provide additional insights into the relationship between Sn segregation and GB type. HAGBs were the primary sites for Sn enrichment, while Σ3 twin boundaries, with their low energy and high symmetry, showed no Sn segregation. This selective segregation behavior is comparable to studies on Mg alloys, where high-energy GBs were preferred sites for solute segregation due to their higher interface energy [36, 37]. After annealing at 350 °C, both the slight increase in lattice parameter (Figure 2b) and the asymmetric Sn cloud close to some GBs (Figure S9) indicate that Sn was removed from the GB during grain growth and incorporated into the crystal lattice.

The STEM analysis revealed no noticeable variation in the dislocation content within the grain interior before and after annealing as shown in Fig. 3 (a) and (b). This observation might suggest that the annihilation of mobile dislocations does not play a major role. However, it is important to note that quantifying dislocation density in nanocrystalline materials still remains challenging. Since the measured KAM values (supplementary Fig. S7) are based on the orientation variation and are quite sensitive to grain overlap in the ACOM maps, especially at GBs, the numerical difference is not a reliable indicator for the dislocation density in nanocrystalline materials. Nevertheless, the KAM maps indicate that no significant dislocation activity occurs during annealing at 200 °C. Nevertheless, while the current data do not strongly support dislocation-related mechanisms, their subtle contributions cannot be entirely ruled out. Nevertheless, a reduction of mobile dislocation density occurs because NC/UFG materials have a high density of grain boundaries, which provide numerous dislocation sinks [38]. During annealing, these grain boundaries effectively absorb and annihilate stored dislocations. Thus, higher stresses are required to activate new dislocation sources in order to realize plastic deformation [39]. Once a certain amount of plastic strain is introduced, the density of mobile dislocations increases and the hardening effect diminishes. This phenomenon is often referred to as “hardening by annealing and softening by deformation” [40]. This behavior also fits to the observed increase in pile-up around the indentation. Due to induced softening by indentation within the plastically deformed volume, the material flow is localized on the surface, leading to an enhanced pile-up. Similar effects were observed for HPT deformed Cantor alloys [41].

Grain boundary relaxation occurs during annealing leading to more energetically favorable GB structures, which make it more difficult to emit dislocations. This also results in higher stresses required for initiating dislocations, thereby contributing to the enhanced strength of annealed NC/UFG materials [42-44]. The exothermic peak between 120 °C and 230 °C in the DSC curve (supplementary Fig. S8) corresponds to the strain release, a phenomenon observed in other FCC nanocrystalline materials, such as nanostructured Cu [45, 46], where GB relaxation precedes grain growth. Molecular dynamics simulations have also shown that high-energy GBs tend to relax by emitting partial dislocations, which reduces GB energy and increases the stress needed for dislocation emission [47]. This stabilizing effect at the GBs is consistent with studies on nanostructured Ni, where GB relaxation raises the activation barrier for dislocation slip, requiring higher stresses to initiate deformation. Similar behavior has been observed in Cu-8 wt.% Sn, where Zaher et al. [19] noted a higher recrystallization temperature and activation energy for recrystallization compared to pure Cu. This is attributed to the strong interaction between Sn atoms and GBs, which slows down recrystallization and stabilizes the microstructure.

In summary, the hardening observed in CuSn5 upon annealing up to 200 °C arises from GB relaxation. Selective Sn segregation at HAGBs enhances GB stability and improves resistance to deformation. This mechanism supports the effectiveness of solute segregation in stabilizing NC/UFG structures. However, at 350 °C, grain coarsening reduces HAGB density, pushing Sn to reintegrate into the matrix, which decreases boundary strengthening and contributes to the observed decrease in hardness. These findings highlight the role of Sn segregation in enhancing the thermal stability of CuSn5, comparable to effects observed in similar alloy systems.

5. Conclusion

This study investigated the thermal stability and hardening mechanisms in NC/UFG CuSn5 alloy processed by high-pressure torsion (HPT) and subsequently annealed at temperatures up to 350 °C. Our findings demonstrate that Sn segregation at grain boundaries (GBs), particularly random high-angle grain boundaries (HAGBs), plays a crucial role in stabilizing the UFG structure and enhancing hardness at moderate annealing temperatures. The key conclusions are summarized as follows:

1. Enhanced hardness through HPT and annealing: HPT significantly increases the hardness of the alloy by reducing its grain size. The further increase in hardness after annealing up to 200°C is attributed to GB relaxation and selective Sn segregation at random high-angle

grain boundaries (HAGBs), which hinder GB migration. Beyond 200 °C, the hardness gradually declines due to solute redistribution and grain growth.

2. Segregation Mechanism: STEM-EDS in combination with 4D-STEM orientation mapping confirmed preferential Sn segregation at general HAGBs, while low-angle grain boundaries (LAGBs), and Σ3 twin boundaries show minimal Sn enrichment. This segregation behavior is consistent with the higher energy of random HAGBs, making them favorable sites for solute atoms. The presence of Sn at HAGBs contributes to boundary stabilization and impedes dislocation emission, effectively raising the stress needed for plastic deformation and enhancing the hardness of the alloy.

In conclusion, Sn segregation at HAGBs is the dominant mechanism behind the annealing-induced hardening and thermal stability observed in HPT-processed CuSn5. These insights offer valuable guidance for designing nanostructured alloys with enhanced mechanical performance and thermal reliability, particularly for applications requiring a combination of high strength and thermal stability without complex phase evolution.

Declaration of competing interest

The authors declare that they have no known competing financial interests or personal relationships that could have appeared to influence the work reported in this paper.

CRediT authorship contribution statement

Yuting Dai: Writing-original draft, Writing-review & editing, Visualization, Validation, Investigation, Data curation, Formal analysis. **Ali Ahmadian**: Writing-review & editing, Conceptualization. **Oliver Petry**: Writing-review & editing, Validation, Methodology, Investigation. **Marcel Sos**: Writing-review & editing, Validation, Methodology, Investigation. **Matthias Schwotzer**: Writing-review & editing, Methodology, Investigation. **Karsten Durst**: Writing-review & editing, Supervision, Resources, Project administration, Methodology, Funding acquisition, Conceptualization. **Christian Kübel**: Writing-review & editing, Supervision, Methodology, Funding acquisition, Conceptualization.

Acknowledgement

Y. Dai acknowledges the China Scholarship Council (CSC) and support from Deutsche Forschungsgemeinschaft (DFG) through the CRC 1441 TrackAct for supporting his Ph.D. at the Karlsruhe Institute of Technology and Technical University Darmstadt. M.S., O.P., K.D. acknowledge support from Deutsche Forschungsgemeinschaft (DFG) for partial funding of this

work. We acknowledge support by the KIT-Publication Fund of the Karlsruhe Institute of Technology.

Appendix A. Supplementary data

The following are the Supplementary data to this article:

Data availability

Research data associated with this article is available on KITOpen under DOI:

References

[1] E. Hall, The deformation and ageing of mild steel: III discussion of results, Proceedings of the Physical Society. Section B, 64(9) (1951) 747-752.http://doi.org/10.1088/0370-1301/64/9/303.
[2] N.J. Petch, The cleavage strength of polycrystals, J. Iron Steel Inst., 174 (1953) 25-28.
[3] Y. Estrin, A. Vinogradov, Extreme grain refinement by severe plastic deformation: A wealth of challenging science, Acta Materialia, 61(3) (2013) 782-817.http://doi.org/10.1016/j.actamat.2012.10.038.
[4] Y. Chen, N. Gao, G. Sha, S.P. Ringer, M.J. Starink, Microstructural evolution, strengthening and thermal stability of an ultrafine-grained Al–Cu–Mg alloy, Acta Materialia, 109 (2016) 202-212.http://doi.org/10.1016/j.actamat.2016.02.050.
[5] M. Kawasaki, Different models of hardness evolution in ultrafine-grained materials processed by high-pressure torsion, Journal of Materials Science, 49(1) (2013) 18-34.http://doi.org/10.1007/s10853-013-7687-9.
[6] D.P. Shen, H.B. Zhou, W.P. Tong, Influence of deformation temperature on the microstructure and thermal stability of HPT-consolidated Cu-1%Nb alloys, Journal of Materials Research and Technology, 8(6) (2019) 6396-6399.http://doi.org/10.1016/j.jmrt.2019.09.054.
[7] Y. Huang, S. Sabbaghianrad, A.I. Almazrouee, K.J. Al-Fadhalah, S.N. Alhajeri, T.G. Langdon, The significance of self-annealing at room temperature in high purity copper processed by high-pressure torsion, Materials Science and Engineering: A, 656 (2016) 55-66.http://doi.org/10.1016/j.msea.2016.01.027.
[8] K. Edalati, D. Akama, A. Nishio, S. Lee, Y. Yonenaga, J.M. Cubero-Sesin, Z. Horita, Influence of dislocation–solute atom interactions and stacking fault energy on grain size of single-phase alloys after severe plastic deformation using high-pressure torsion, Acta Materialia, 69 (2014) 68-77.http://doi.org/10.1016/j.actamat.2014.01.036.
[9] E. Bruder, P. Braun, H.u. Rehman, R.K.W. Marceau, A.S. Taylor, R. Pippan, K. Durst, Influence of solute effects on the saturation grain size and rate sensitivity in Cu-X alloys, Scripta Materialia, 144 (2018) 5-8.http://doi.org/10.1016/j.scriptamat.2017.09.031.
[10] T. Keil, C. Minnert, E. Bruder, K. Durst, Solid solution hardening effects on structure evolution and mechanical properties of nanostructured binary and high entropy alloys after high pressure torsion, IOP Conference Series: Materials Science and Engineering, 1249(1) (2022) 012003.http://doi.org/10.1088/1757-899X/1249/1/012003.
[11] K. Edalati, J.M. Cubero-Sesin, A. Alhamidi, I.F. Mohamed, Z. Horita, Influence of severe plastic deformation at cryogenic temperature on grain refinement and softening of pure metals: Investigation using high-pressure torsion, Materials Science and Engineering: A, 613 (2014) 103-110.http://doi.org/10.1016/j.msea.2014.06.084.
[12] N. Liang, Y. Zhao, Y. Li, T. Topping, Y. Zhu, R.Z. Valiev, E.J. Lavernia, Influence of microstructure on thermal stability of ultrafine-grained Cu processed by equal channel

angular pressing, Journal of Materials Science, 53(18) (2018) 13173-13185.http://doi.org/10.1007/s10853-018-2548-1.
[13] E. Schafler, M.B. Kerber, Microstructural investigation of the annealing behaviour of high-pressure torsion (HPT) deformed copper, Materials Science and Engineering: A, 462(1-2) (2007) 139-143.http://doi.org/10.1016/j.msea.2005.11.085.
[14] C. Minnert, K. Durst, Nanoindentation creep testing: Advantages and limitations of the constant contact pressure method, Journal of Materials Research, 37(2) (2021) 567-579.http://doi.org/10.1557/s43578-021-00445-6.
[15] G. Gottstein, L.S. Shvindlerman, Grain boundary migration in metals: thermodynamics, kinetics, applications, 2nd ed., CRC press, Boca Raton,2009.
[16] K.A. Darling, M.A. Tschopp, B.K. VanLeeuwen, M.A. Atwater, Z.K. Liu, Mitigating grain growth in binary nanocrystalline alloys through solute selection based on thermodynamic stability maps, Computational Materials Science, 84 (2014) 255-266.http://doi.org/10.1016/j.commatsci.2013.10.018.
[17] M.A. Atwater, R.O. Scattergood, C.C. Koch, The stabilization of nanocrystalline copper by zirconium, Materials Science and Engineering: A, 559 (2013) 250-256.http://doi.org/10.1016/j.msea.2012.08.092.
[18] T. Meiners, J.M. Duarte, G. Richter, G. Dehm, C.H. Liebscher, Tantalum and zirconium induced structural transitions at complex [111] tilt grain boundaries in copper, Acta Materialia, 190 (2020) 93-104.http://doi.org/10.1016/j.actamat.2020.02.064.
[19] G. Zaher, I. Lomakin, N. Enikeev, S. Jouen, A. Saiter-Fourcin, X. Sauvage, Influence of strain rate and Sn in solid solution on the grain refinement and crystalline defect density in severely deformed Cu, Materials Today Communications, 26 (2021) 101746.http://doi.org/10.1016/j.mtcomm.2020.101746.
[20] D. Wang, Y. Li, B. Sun, M. Sui, K. Lu, E. Ma, Bulk metallic glass formation in the binary Cu–Zr system, Applied Physics Letters, 84(20) (2004) 4029-4031.http://doi.org/10.1063/1.1751219.
[21] A. Khalajhedayati, T.J. Rupert, High-temperature stability and grain boundary complexion formation in a nanocrystalline Cu-Zr alloy, JOM, 67 (2015) 2788-2801.http://doi.org/10.1007/s11837-015-1644-9.
[22] E. Nes, N. Ryum, O. Hunderi, On the Zener drag, Acta metallurgica, 33(1) (1985) 11-22.http://doi.org/10.1016/0001-6160(85)90214-7.
[23] W.C. Oliver, G.M. Pharr, An improved technique for determining hardness and elastic modulus using load and displacement sensing indentation experiments, Journal of Materials Research, 7(6) (1992) 1564-1583.http://doi.org/10.1557/JMR.1992.1564.
[24] I.V. Alexandrov, Microstructural characterization of SPD processed materials, Metals and Materials International, 7 (2001) 565-571.http://doi.org/10.1007/BF03179255.
[25] M. Sos, G. Tiphene, J.-L. Loubet, S. Bruns, E. Bruder, K. Durst, Mechanical softening of CuX alloys at elevated temperatures studied via high temperature scanning indentation, Materials & Design, 240 (2024) 112865.http://doi.org/10.1016/j.matdes.2024.112865.
[26] A. Kobler, C. Kubel, Challenges in quantitative crystallographic characterization of 3D thin films by ACOM-TEM, Ultramicroscopy, 173 (2017) 84-94.http://doi.org/10.1016/j.ultramic.2016.07.007.
[27] A. Kobler, A. Kashiwar, H. Hahn, C. Kübel, Combination of in situ straining and ACOM TEM: A novel method for analysis of plastic deformation of nanocrystalline metals, Ultramicroscopy, 128 (2013) 68-81.http://doi.org/10.1016/j.ultramic.2012.12.019.
[28] J. Duan, H. Wen, C. Zhou, X. He, R. Islamgaliev, R. Valiev, Discontinuous grain growth in an equal-channel angular pressing processed Fe-9Cr steel with a heterogeneous microstructure, Materials Characterization, 159 (2020).http://doi.org/10.1016/j.matchar.2019.110004.

[29] C. Liu, X. Chen, D. Tolnai, Y. Hu, W. Zhang, Y. Zhang, F. Pan, Annealing hardening effect aroused by solute segregation in gradient ultrafine-grained Mg-Gd-Zr alloy, Journal of Materials Science & Technology, 144 (2023) 70-80.http://doi.org/10.1016/j.jmst.2022.10.015.
[30] T. Frolov, K.A. Darling, L.J. Kecskes, Y. Mishin, Stabilization and strengthening of nanocrystalline copper by alloying with tantalum, Acta Materialia, 60(5) (2012) 2158-2168.http://doi.org/10.1016/j.actamat.2012.01.011.
[31] J. Tao, G. Chen, W. Jian, J. Wang, Y. Zhu, X. Zhu, T.G. Langdon, Anneal hardening of a nanostructured Cu–Al alloy processed by high-pressure torsion and rolling, Materials Science and Engineering: A, 628 (2015) 207-215.http://doi.org/10.1016/j.msea.2015.01.055.
[32] J. Yang, Y. Pang, P. Li, Z. Yin, Y. Gong, X. Zhu, The Anneal Hardening and Deformation Softening Behaviors of Nanocrystalline Cu-Zn Alloys, Materials Transactions, 57(8) (2016) 1261-1265.http://doi.org/10.2320/matertrans.MG201618.
[33] I. Marković, S. Ivanov, U. Stamenković, R. Todorović, A. Kostov, Annealing behavior of Cu-7at.%Pd alloy deformed by cold rolling, Journal of Alloys and Compounds, 768 (2018) 944-952.http://doi.org/10.1016/j.jallcom.2018.07.258.
[34] I. Marković, S. Nestorović, B. Markoli, M. Premović, S. Šturm, Anneal hardening in cold rolled PM Cu-Au alloy, Materials Science and Engineering: A, 658 (2016) 393-399.http://doi.org/10.1016/j.msea.2016.02.029.
[35] J. Gubicza, Annealing - Induced Hardening in Ultrafine - Grained and Nanocrystalline Materials, Advanced Engineering Materials, 22(1) (2019) 1900507.http://doi.org/10.1002/adem.201900507.
[36] Y.M. Zhu, S.W. Xu, J.F. Nie, {101¯1} Twin boundary structures in a Mg–Gd alloy, Acta Materialia, 143 (2018) 1-12.http://doi.org/10.1016/j.actamat.2017.09.067.
[37] T. Tsuru, H. Somekawa, D.C. Chrzan, Interfacial segregation and fracture in Mg-based binary alloys: Experimental and first-principles perspective, Acta Materialia, 151 (2018) 78-86.http://doi.org/10.1016/j.actamat.2018.03.061.
[38] J. Kacher, B.P. Eftink, B. Cui, I.M. Robertson, Dislocation interactions with grain boundaries, Current Opinion in Solid State and Materials Science, 18(4) (2014) 227-243.http://doi.org/10.1016/j.cossms.2014.05.004.
[39] Y. Bai, H. Kitamura, S. Gao, Y. Tian, N. Park, M.H. Park, H. Adachi, A. Shibata, M. Sato, M. Murayama, N. Tsuji, Unique transition of yielding mechanism and unexpected activation of deformation twinning in ultrafine grained Fe-31Mn-3Al-3Si alloy, Scientific Reports, 11(1) (2021) 15870.http://doi.org/10.1038/s41598-021-94800-6.
[40] X. Huang, N. Hansen, N. Tsuji, Hardening by annealing and softening by deformation in nanostructured metals, Science, 312(5771) (2006) 249-251.http://doi.org/10.1126/science.1124268.
[41] T. Keil, S. Taheriniya, E. Bruder, G. Wilde, K. Durst, Effects of solutes on thermal stability, microstructure and mechanical properties in CrMnFeCoNi based alloys after high pressure torsion, Acta Materialia, 227 (2022) 117689.http://doi.org/10.1016/j.actamat.2022.117689.
[42] A.v. Hasnaoui, H. Van Swygenhoven, P. Derlet, On non-equilibrium grain boundaries and their effect on thermal and mechanical behaviour: a molecular dynamics computer simulation, Acta Materialia, 50(15) (2002) 3927-3939.http://doi.org/10.1016/S1359-6454(02)00195-7.
[43] G.J. Tucker, D.L. McDowell, Non-equilibrium grain boundary structure and inelastic deformation using atomistic simulations, International Journal of Plasticity, 27(6) (2011) 841-857.http://doi.org/10.1016/j.ijplas.2010.09.011.

[44] I.A. Ovid'ko, A.G. Sheinerman, R.Z. Valiev, Dislocation emission from deformation-distorted grain boundaries in ultrafine-grained materials, Scripta Materialia, 76 (2014) 45-48.http://doi.org/10.1016/j.scriptamat.2013.12.012.
[45] Y.A. Sun, Z.P. Luo, X.Y. Li, K. Lu, Effects of stacking fault energy on deformation induced grain boundary relaxation in nanograined Cu alloys, Acta Materialia, 239 (2022) 118256.http://doi.org/10.1016/j.actamat.2022.118256.
[46] X. Zhou, X. Li, K. Lu, 70 nm: The most unstable grain size in Cu prepared by surface mechanical grinding treatment, Nano Materials Science, 2(1) (2020) 32-38.http://doi.org/10.1016/j.nanoms.2020.01.001.
[47] V. Yamakov, D. Wolf, S.R. Phillpot, A.K. Mukherjee, H. Gleiter, Deformation-mechanism map for nanocrystalline metals by molecular-dynamics simulation, Nature Materials, 3(1) (2004) 43-47.http://doi.org/10.1038/nmat1035.

Declaration of competing interests

The authors have nothing to declare.

Highlights

1. Grain growth behavior of ultrafine-grained Cu-5 wt.% Sn was systematically studied.
2. Sn atoms preferentially segregate at general high-angle grain boundaries.
3. No detectable Sn segregation was found at LAGBs and CSL boundaries.
4. Grain boundary segregation and relaxation enhanced Vickers hardness after low temperature annealing.